Probing the nuclear interaction radius with single-proton transfer reactions*

Runlong Liu (刘润龙)[1] Shengquan Yan (颜胜权)[1†] Yunju Li (李云居)[1] Peiwei Wen (温培威)[1]
Xinyue Li (李鑫悦)[3] Katsuhisa Nishio[2] Youbao Wang (王友宝)[1] Zhihong Li (李志宏)[1]
Ertao Li (李二涛)[4] Hiroyuki Makii[2] Riccardo Orlandi[2] Guangshun Li (李广顺)[3]
Jianguo Wang (王建国)[3] Bingshui Gao (高丙水)[3] Yangping Shen (谌阳平)[1]
Jie Ren (任杰)[1] Qiwen Fan (樊启文)[1] Sheng Zeng (曾晟)[1] Wei Nan (南巍)[1]
Chen Chen (陈晨)[1] Gang Lian (连钢)[1] Bing Guo (郭冰)[1‡]

[1]China Institute of Atomic Energy, P.O. Box 275(10), Beijing 102413, China
[2]Advanced Science Research Center, Japan Atomic Energy Agency, Tokai, Ibaraki 319-1195, Japan
[3]Institute of Modern Physics, Chinese Academy of Sciences, Lanzhou 730000, China
[4]Institute for Advanced Study in Nuclear Energy & Safety, College of Physics and Optoelectronic Engineering, Shenzhen University, Shenzhen 518060, China

Abstract: In this work, the ^{56,58}Fe(^{18}O,^{17}N)^{57,59}Co transfer reactions were measured, and Distorted Wave Born Approximation calculations using the systematic heavy-ion optical potential were employed to reproduce the experimental data and investigate the interaction radius. The Coulomb barrier radii r_B were determined to be 9.58 ± 0.35 fm and 9.83 ± 0.37 fm for ^{18}O+^{56}Fe and ^{18}O+^{58}Fe, respectively. The maximum distances between the surfaces of the two nuclei were calculated to be 0.68 ± 0.35 fm for ^{18}O + ^{56}Fe and 0.85 ± 0.37 fm for ^{18}O + ^{58}Fe. These results provide a clear physical picture of the distance between the surfaces of the two nuclei in single-nucleon transfer reactions.

Keywords: interaction radius, Distorted Wave Born Approximation, single-proton transfer reaction

DOI: 10.1088/1674-1137/ae7ff6 **CSTR:** 32044.14.ChinesePhysicsC.50094004

I. INTRODUCTION

In heavy-ion collisions above the Coulomb barrier, reactions in which the projectile loses only a moderate amount of energy and exchanges only a few nucleons with the target nucleus are assumed to occur when the two ions make grazing contact at their surfaces. Single-nucleon transfer reactions typically occur when nuclear surfaces approach distances at which the tails of the two wavefunctions begin to overlap in the attractive nuclear field [1]. Accordingly, single-nucleon transfer reactions are inherently sensitive to the tails of the nuclear wavefunctions and, consequently, to the radius and diffuseness of the nuclear potential. Because single-nucleon transfer is a direct, one-step reaction, Distorted Wave Born Approximation (DWBA) calculations [2−4] can be employed to extract the optical potential parameters, from which the interaction radius can be determined [5−8]. As a key parameter, the interaction radius characterizes the distance scale at which two nuclei begin to interact and provides critical insight into the nuclear potential and collision geometry. In this work, single-proton transfer reactions ^{56,58}Fe(^{18}O,^{17}N)^{57,59}Co were carried out, and DWBA calculations were employed to reproduce the experimental data using the systematic optical potential for heavy ions [9] to investigate the interaction radii. The obtained results were then compared with the radii extracted from Refs. [7, 10−14].

II. EXPERIMENT SETUP

The experiments were carried out at the Tandem Accelerator of the Japan Atomic Energy Agency (JAEA). An ^{18}O beam with an incident energy of 103.0 MeV was directed onto metallic self-supporting iron foil targets. The ^{56}Fe target was 402 μg/cm^2 thick, with an isotopic

Received 7 April 2026; Accepted 22 June 2026; Accepted manuscript online 23 June 2026

* This work was supported by the National Natural Science Foundation of China (12125509, 12435010, 12441507, U2441220, U2541244, 12175152, 12505160, 12475151, 12405164), the National Key Research and Development Project (2022YFA1602301). The CNNC Science Fund for Talented Young Scholars, The CNNC Fundamental Research Project

† E-mail: panyu@ciae.ac.cn
‡ E-mail: guobing@ciae.ac.cn

enrichment of 99.4%, whereas the ^{58}Fe target had a thickness of 260 μg/cm^2 and an isotopic enrichment of 96.3%. An array of $\Delta E-E$ silicon detectors was placed approximately 110 mm downstream of the target to identify light ejectiles. The trapezoidal ΔE detectors were arranged in a ring around the beam axis to collect the scattered ejectiles over an angular range of 12.2°−21.4° relative to the beam direction. The thickness of the ΔE detector was 68 μm. The E detector was an annular detector segmented into 16 ring-shaped strips, allowing the ejectile scattering angle to be determined with an angular resolution of approximately 0.6°. The E detector had a thickness of 300 μm. Four HPGe detectors were mounted perpendicular to the beam axis for measurements of the ^{56,58}Fe(^{18}O,^{16}Oγ)^{58,60}Fe reactions [15]. A Faraday cup was installed approximately 1.3 m downstream of the target to integrate the ^{18}O beam dose. The average intensity of the ^{18}O beam was approximately 0.2 pnA, and the diameter of the beam spot was less than 3 mm. Each Fe target was irradiated for approximately 2.5 days, and the total accumulated numbers of ^{17}N were approximately 9.2×10^5 and 1.0×10^6 for the ^{56}Fe and ^{58}Fe targets, respectively.

III. DATA ANALYSIS

Particle identification was performed using the two-dimensional $\Delta E-E_t$ spectrum collected with the $\Delta E-E$ silicon telescope, where E_t is the total energy, defined as the sum of the energy loss in the ΔE detector and the residual energy deposited in the annular E detector. As an example, the $\Delta E-E_t$ scatter plot obtained from one ΔE detector and the fifth inner strip of the annular E detector is shown in Fig. 1. A cut was applied to select ^{17}N events from the ^{58}Fe(^{18}O,^{17}N)^{59}Co proton transfer reaction. Because the first excited-state energies of ^{17}N and ^{57,59}Co are 1373.9, 1224.0, and 1099.3 keV, respectively, the ^{17}N ground state can be clearly separated and identified in the $\Delta E-E_t$ two-dimensional spectrum. Within the selected cut, ^{17}N and ^{59}Co are both in their ground states, as determined from the reaction kinematics. The energy resolution for ^{17}N is approximately 0.5 MeV in full width at half maximum (FWHM), dominated by the noise of the silicon detectors and the angular uncertainty arising from the ~0.6° acceptance of each ring.

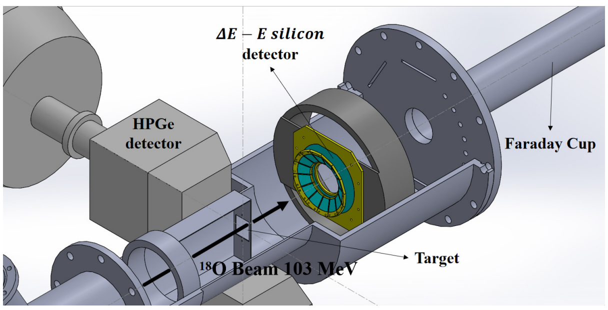

Fig. 1. (color online) Experimental Setup.

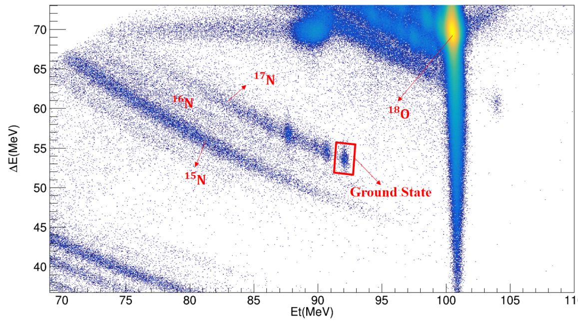

Fig. 2. (color online) $\Delta E-E_t$ two-dimensional spectrum of the products from ^{18}O+^{58}Fe. A cut is set to select the (^{18}O,^{17}N) events where ^{17}N and ^{59}Co are both in ground states.

After the ^{17}N events were obtained for each strip of the annular E detector in the ^{56,58}Fe(^{18}O,^{17}N)^{57,59}Co reactions, the angular distributions for the ground-state transitions to ^{59}Co and ^{57}Co were extracted, as shown in Fig. 2. The $\Delta E-E$ silicon telescope covered laboratory angles of 12.2°−21.4°, corresponding to 16.5°−27.6° in the center-of-mass (c.m.) frame. This angular range includes the main peaks of the proton-transfer angular distributions, as the grazing angles for the ^{56,58}Fe(^{18}O,^{17}N)^{57,59}Co reactions are approximately 21° (c.m.), as shown in Fig. 3. Angular uncertainties are dominated by the ~0.6° angular bin size of the individual E detector strips. The reported cross-section uncertainties include statistical contributions and background-subtraction uncertainties.

To extract the optical potential parameters for the ^{56,58}Fe(^{18}O,^{17}N)^{57,59}Co reactions, DWBA calculations were performed using the PTOLEMY [16] code to reproduce the measured angular distributions of these transfer reactions. The calculated results are shown in Fig. 3. The optical potential parameters for the entrance channels (^{18}O+^{56,58}Fe) and exit channels (^{17}N+^{57,59}Co) were taken from the systematic optical model potential reported in Ref. [9].

In Ref. [9], the parameters R and a for the systematic heavy-ion optical potential used in DWBA calculations were determined using Eq. (1):

$$\begin{aligned} R_V = R_W &= (1.772\pm0.039)\times(A_1^{1/3}+A_2^{1/3}) \\ &\quad -(4.881\pm0.256), \\ a_V = a_W &= (-0.0736\pm0.011)\times(A_1^{1/3}+A_2^{1/3}) \\ &\quad +(1.087\pm0.063). \end{aligned} \tag{1}$$

A_1 and A_2 are the mass numbers of the projectile and target nuclei, respectively. The real part V and imaginary part W of the optical potential depth were determined using the energy dispersion relation parameter (EDRP) in

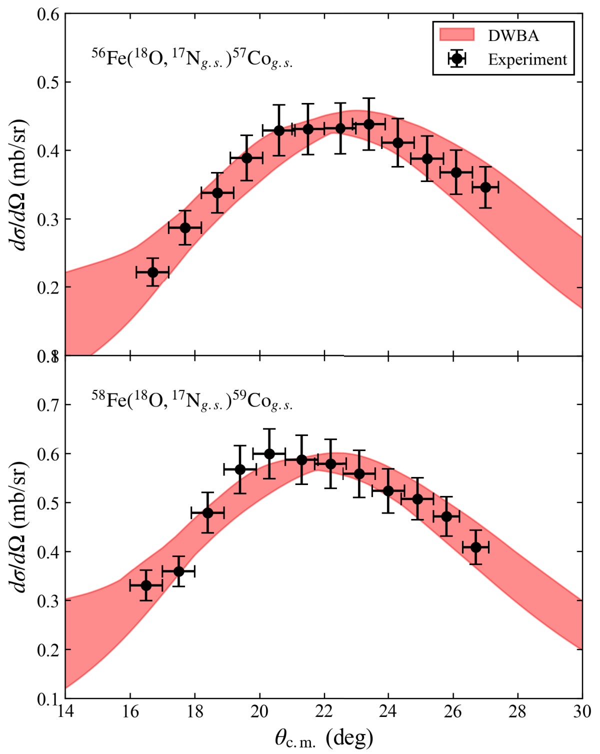

Fig. 3. (color online) The angular distributions of $^{56}Fe(^{18}O,^{17}N_{g.s.})^{57}Co_{g.s.}$ and $^{58}Fe(^{18}O,^{17}N_{g.s.})^{59}Co_{g.s.}$ reactions. The black solid circles are the experimental data, the DWBA calculations are red bands. The spectroscopic factors of these two reactions are 0.10 ± 0.06 for $^{56}Fe(^{18}O,^{17}N_{g.s.})^{57}Co_{g.s.}$ and 0.14 ± 0.08 for $^{58}Fe(^{18}O,^{17}N_{g.s.})^{59}Co_{g.s.}$.

Eq. (2):

$$\begin{aligned} &V = 268.7\pm24.1,\\ &EDRP = E_{\rm lab}\times(A_1^{1/3}+A_2^{1/3})/Z_1Z_2,\\ &W/V = \begin{cases} 0.0416\times EDRP+0.4124 & EDRP<10,\\ 0.8284 & EDRP\geq 10. \end{cases} \end{aligned} \tag{2}$$

$E_{\rm lab}$ is the projectile energy, and Z_1 and Z_2 are the charge numbers of the projectile and target nuclei, respectively. To optimize the optical model parameters, V, R_V, and a were adjusted within the ranges given in Eq. (1) and Eq. (2) so that the theoretical results reproduced the experimental data. The optical potential parameters corresponding to a one-σ deviation between the theoretical and experimental values were defined as a set, thereby determining the parameter range for each optical potential. The parameters are listed in Table 1. The bound-state potential parameters were set identically for the respective nuclei. For ^{18}O, ^{56}Fe, and ^{58}Fe, the single-particle state parameters were fixed at r_0 = 1.25 fm, a_0 = 0.65 fm, and $V_{\rm s.o.}$ = 6.0 MeV. The potential depth V was subsequently varied within the range of 50−70 MeV to reproduce the respective bound states. These parameter settings were adopted from Refs. [17−19]. The spectroscopic factors (SFs) for both reactions were extracted by fitting the DWBA calculations to the experimental angular distributions using the least-squares method. The experimental SF was determined to be 0.10 ± 0.06 for the $^{56}Fe(^{18}O,^{17}N_{g.s.})^{57}Co_{g.s.}$ reaction and 0.14 ± 0.08 for the $^{58}Fe(^{18}O,^{17}N_{g.s.})^{59}Co_{g.s.}$ reaction.

Single-nucleon transfer reactions occur in grazing collisions at the nuclear surface. Therefore, the effective interaction radii can be identified with the grazing radii $r_{\rm g}$. First, the total effective potential $U_{\rm eff}(r)$ can be calculated using the obtained optical potential parameters:

$$U_{\rm eff}(r) = V_N(r)+V_C(r)+\frac{\hbar^2L(L+1)}{2\mu r^2}. \tag{3}$$

where $V_N(r)$ is the nuclear potential, $V_C(r)$ is the Coulomb potential, and $\frac{\hbar^2L(L+1)}{2\mu r^2}$ is the angular-momentum-dependent term. Here, L is the angular momentum, and μ is the reduced mass of the system. When $L=0$, the Coulomb barrier radius $r_{\rm B}$ can be deduced from Eq. (4). The calculated values of $r_{\rm B}$ are 9.58 ± 0.35 fm for $^{18}O+^{56}Fe$ and 9.83 ± 0.37 fm for $^{18}O+^{58}Fe$.

$$\left.\frac{\partial U_{\rm eff}(r)}{\partial r}\right|_{r=r_{\rm B}} = 0. \tag{4}$$

The grazing radius $r_{\rm g}$ can then be determined from Eq. (5) in Ref. [1] by setting $L=L_{\rm g}$.

Table 1. OMPs used In DWBA for reaction channels.

Channel	$E_{\rm lab}$/MeV	V/MeV	W/V	r_0/fm	a_0/fm
$^{18}O+^{56}Fe$	103.00	281.5 ± 7.1	0.545	1.030 ± 0.027	0.590 ± 0.065
$^{17}N+^{57}Co$	88.33	277.5 ± 8.4	0.537	0.953 ± 0.015	0.590 ± 0.042
$^{18}O+^{58}Fe$	103.00	282.4 ± 7.1	0.546	1.052 ± 0.029	0.599 ± 0.066
$^{17}N+^{59}Co$	90.21	277.9 ± 8.4	0.541	0.952 ± 0.010	0.563 ± 0.040

$$
\begin{aligned}
&E_{\text{c.m.}} - (U_{\text{eff}}(r_{\text{g}}))_{L=L_{\text{g}}} = 0, \\
&\left.\frac{\partial U_{\text{eff}}(r)}{\partial r}\right|_{r=r_{\text{g}},L=L_{\text{g}}} = 0.
\end{aligned} \tag{5}
$$

Using the equations above, the total effective potentials of $^{18}\text{O}+^{56,58}\text{Fe}$ at 103 MeV were calculated, and the results are shown in Fig. 4. The grazing radii r_{g} were determined to be 8.59 ± 0.23 fm and 8.80 ± 0.25 fm for $^{18}\text{O}+^{56}\text{Fe}$ and $^{18}\text{O}+^{58}\text{Fe}$, respectively. Because the grazing radius corresponds to the position where the projectile's kinetic energy equals the potential energy, it effectively serves as the turning point [20], marking the classical distance of closest approach. However, r_{g} increases as the incident energy of ^{18}O decreases, and the cross section of the single-proton transfer reaction decreases sharply when the incident energy of ^{18}O falls below the Coulomb barrier. Thus, r_{g} for the two reactions reaches its maximum values, corresponding to the values of r_{B} mentioned above.

IV. DISCUSSION

The nuclear interaction radius defines the characteristic distance at which nuclear forces become appreciable and governs the probability of direct processes, such as single-nucleon transfer, which occur predominantly near this radius. Thus, this radius determines the grazing trajectory of reactions, and its signature is encoded in experimental observables, such as angular distributions and excitation functions, making it a fundamental quantity in the analysis of reaction mechanisms. Accordingly, considerable effort has been devoted to estimating this radius, including the Bass80 [11], CW76 [13], BW91 [11, 21], and AW95 [12] models. In this work, the Coulomb barrier radii r_{B} for these proximity potential models were calculated for comparison with the values obtained in the present study. The CW76 and AW95 models were developed from extensive experimental data on heavy-ion collisions and scattering and provide empirical formulas for calculating r_{B}. The formulas are given as:

$$
\begin{aligned}
r_{\text{B}}^{\text{CW76}} &= 1.07(A_1^{1/3}+A_2^{1/3})+2.72, \\
r_{\text{B}}^{\text{AW95}} &= 1.08(A_1^{1/3}+A_2^{1/3})+1.20 \\
&\quad +0.34(28.6-A_1^{1/3}A_2^{1/3})^{1/2}.
\end{aligned} \tag{6}
$$

For the Bass80 and BW91 models, no empirical formula is available for r_{B}. Consequently, r_{B} is determined from their respective nuclear potentials. The nuclear potential for the Bass80 model is formulated as follows:

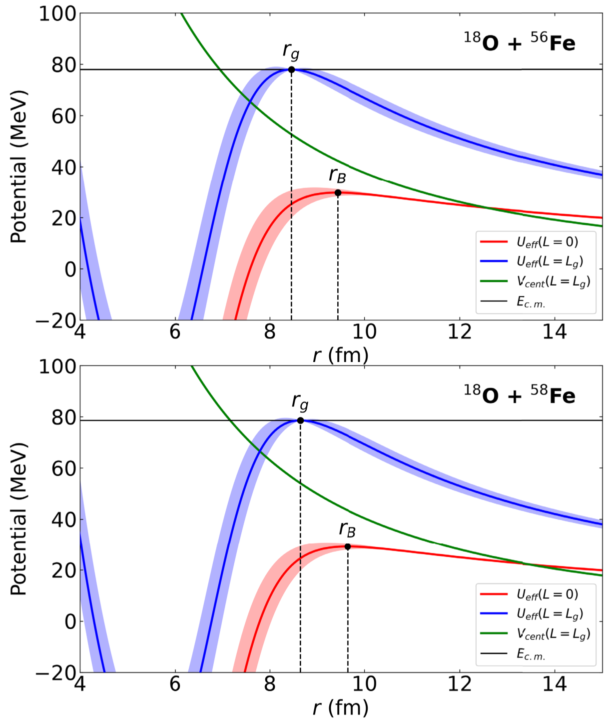

Fig. 4. (color online) The U_{eff} of the incident system $^{18}\text{O}+^{56,58}\text{Fe}$. The blue line and its shaded band represent U_{eff} with the grazing angular momentum L_{g} at the 103 MeV incident energy. The red line and its shaded band represent U_{eff} with the angular momentum $L=0$. The r_{B} and r_{g} are Coulomb barrier radii and grazing radii of $^{18}\text{O}+^{56,58}\text{Fe}$ channels. The black and green solid line represent the incident center-of-mass energies $E_{\text{c.m.}}$ in measurement and centrifugal potential, respectively.

$$
\begin{aligned}
&U_{\text{N}}^{\text{Bass80}}(r) = -\bar{R}\Phi(s), \\
&\Phi(s) = \left[0.033\exp\left(\frac{r-R_0}{3.5}\right)+0.007\exp\left(\frac{r-R_0}{0.65}\right)\right]^{-1}.
\end{aligned} \tag{7}
$$

Where $\bar{R}$ is the reduced radius of the projectile and target nuclei, and R_0 is the geometric radius. In contrast to the Bass80 potential, the BW91 potential adopts a standard Woods-Saxon form with diffuseness parameter $a=0.63$ fm; the nuclear potential for the BW91 model is expressed as:

$$
U_{\text{N}}^{\text{BW91}}(r) = -\frac{16\pi\bar{R}\gamma a}{1+\exp\left(\dfrac{r-R_0}{a}\right)}. \tag{8}
$$

The definitions of $\bar{R}$ and R_0 are the same as those in the Bass80 model, and γ represents the surface energy coefficient. The r_{B} values calculated for each model and the $r_{\text{B}}^{\text{exp}}$ value obtained in this work are listed in Table 2.

In addition to the proximity potential, r_{B} was also ex-

Table 2. The Coulomb Barrier Radii r_B determined in this work and in different models.

Reaction	r_B^{exp}/fm	r_B^{Bass80}/fm	r_B^{CW76}/fm	r_B^{BW91}/fm	r_B^{AW95}/fm	r_B^{SPP2}/fm
^{56}Fe(^{18}O,^{17}N)^{57}Co	9.58 ± 0.35	9.56	9.62	9.59	9.63	9.60
^{58}Fe(^{18}O,^{17}N)^{59}Co	9.83 ± 0.37	9.64	9.67	9.65	9.67	9.72

tracted from the São Paulo potential calculated using the REGINA code [22] for comparison. Unlike the aforementioned models, the REGINA code employs nucleon density distributions calculated using the Dirac-Hartree-Bogoliubov model to determine the São Paulo potential (SPP2). This approach can calculate both the nuclear potential and the corresponding Coulomb potential of the nuclear system.

The values of r_B estimated by these four models are approximately 9.6 fm. The r_B values extracted in this work are slightly larger on average but agree with the model predictions within experimental uncertainties. Single-nucleon transfer reactions occur when the tails of nuclear potentials overlap, whereas fusion requires the nuclei to approach sufficiently closely for the strong nuclear force to become dominant. Because the proximity potential models are parameterized for fusion reactions, a systematically larger r_B extracted from single-nucleon transfer reactions is consistent with theoretical expectations.

The grazing radii r_g extracted from the systematic heavy-ion optical potential and other potential models are listed in Table 3. For the Bass80, AW76, and BW91 potential models, no solution to Eq. (5) can be obtained. Thus, for these three models, the grazing radii cannot be determined for the reaction systems at an incident energy of 103 MeV. The SPP2 and CW76 potential models do not reproduce the experimental angular distributions accurately. Consequently, the r_g values obtained with the SPP2 and CW76 potentials deviate significantly from those derived from the systematic heavy-ion optical potential.

The single-nucleon transfer reaction is considered to occur on the surfaces of the projectile and target nuclei. Based on the r_B and r_g values obtained in this work, it is useful to discuss the surface distances between the two nuclei near the Coulomb barrier and at an incident energy of 103 MeV for ^{18}O. It is well established that nuclei have diffuse surfaces, where the nucleon density decreases exponentially from 90% to 10% of the central density. The nucleon density distributions obtained with the REGINA code are described by the two-parameter Fermi distribution, and the surface thickness can be calculated from the diffuseness parameter a using Eq. (9):

$$t = 4a\ln 3. \tag{9}$$

By convention, the nuclear surface position is defined as the radius at which the density decreases to 10% of the central density. Therefore, the nuclear surface radius R_s is given by the sum of the half-density radius $R_{1/2}$ and half of the surface thickness t. The nuclear density parameters used in this work are taken from the REGINA code [22]. For ^{18}O, the half-density radius is $R_{p1/2} = 2.57$ fm, and the diffuseness parameter is $a_p = 0.50$ fm. For ^{56}Fe and ^{58}Fe, the half-density radii are $R_{T1/2} = 4.20$ fm and 4.24 fm, respectively; the corresponding diffuseness parameters are $a_T = 0.47$ fm and 0.49 fm. Using the determined value of r_B, the surface distance between the two nuclei can be calculated as $D = r_B - (R_{p1/2} + \frac{1}{2}t_p) - (R_{T1/2} + \frac{1}{2}t_T)$. The resulting values are 0.68 ± 0.35 fm for ^{18}O + ^{56}Fe and 0.85 ± 0.37 fm for ^{18}O + ^{58}Fe. At the higher incident energy of 103 MeV, using r_g, the surface distances are calculated to be -0.31 ± 0.23 fm and -0.19 ± 0.25 fm for the ^{18}O + ^{56}Fe and ^{18}O + ^{58}Fe reactions, respectively. These values indicate that the surface regions of the projectile and target nuclei overlap at 103 MeV. For convenience, the values of the surface distance D are listed in Table 4.

Table 3. The Grazing Radii r_g determined in this work and in different models.

Reaction	r_g^{exp}/fm	r_g^{Bass80}/fm	r_g^{CW76}/fm	r_g^{BW91}/fm	r_g^{AW95}/fm	r_g^{SPP2}/fm
^{56}Fe(^{18}O,^{17}N)^{57}Co	8.59 ± 0.23	*N/A*	8.43	*N/A*	*N/A*	8.28
^{58}Fe(^{18}O,^{17}N)^{59}Co	8.80 ± 0.25	*N/A*	8.49	*N/A*	*N/A*	8.35

Table 4. Surface distance in different reactions.

Reaction	r_B/fm	r_g/fm	$D(r_B)$/fm	$D(r_g)$/fm
^{56}Fe(^{18}O,^{17}N)^{57}Co	9.58 ± 0.35	8.59 ± 0.23	0.68 ± 0.35	−0.31 ± 0.23
^{58}Fe(^{18}O,^{17}N)^{59}Co	9.83 ± 0.37	8.80 ± 0.25	0.85 ± 0.37	−0.19 ± 0.25

V. SUMMARY

In this work, we measured the $^{56,58}Fe(^{18}O,^{17}N)^{57,59}Co$ transfer reactions to investigate nuclear interaction radii. DWBA calculations were used to reproduce the measured angular distributions of these two reactions and to extract optical potential parameters. Using the extracted optical potential parameters, the Coulomb barrier radii r_B were subsequently calculated to be 9.58 ± 0.35 fm for $^{18}O+^{56}Fe$ and 9.83 ± 0.37 fm for $^{18}O+^{58}Fe$. The resulting mean r_B values are slightly larger than the predictions of proximity potential models (Bass80, CW76, BW91, and AW95), but they are consistent with these predictions within experimental uncertainties. The grazing radius r_g was also determined to be 8.59 ± 0.23 fm and 8.80 ± 0.25 fm for $^{18}O+^{56}Fe$ and $^{18}O+^{58}Fe$, respectively, at the experimental incident energy of ^{18}O. Based on the determined radii r_B and r_g, the corresponding surface distances between the two nuclei provide a relatively clear physical picture of the separation between nuclear surfaces in single-nucleon transfer reactions.

References

[1] R. A. Broglia and A. Winther, *Heavy ion reactions: The elementary processes, parts I & II* (Taylor: CRC Press, 2018), p. 128

[2] H. Hasan and C. S. Warke, J. Phys. G: Nucl. Phys. **7**, 1501 (1981)

[3] M. Assunção, R. Lichtenthäler, V. Guimarães *et al*., Phys. Rev. C **70**, 054601 (2004)

[4] W. Henning, Y. Eisen, J. R. Erskine *et al*., Phys. Rev. C **15**, 292 (1977)

[5] H. L. Bradt and B. Peters, Phys. Rev. **77**, 54 (1950)

[6] C. E. Porter, Phys. Rev. **112**, 1722 (1958)

[7] R. Bass, Phys. Lett. B **47**, 139 (1973)

[8] J. S. Blair, Phys. Rev. **95**, 1218 (1954)

[9] L. Gan, Z.-H. Li, H.-B. Sun *et al*., Chin. Phys. C **45**, 054105 (2021)

[10] R. Bass, Phys. Rev. Lett. **39**, 265 (1977)

[11] W. Reisdorf, J. Phys. G: Nucl. Part. Phys. **20**, 1297 (1994)

[12] A. Winther, Nucl. Phys. A **594**, 203 (1995)

[13] P. R. Christensen and A. Winther, Phys. Lett. B **65**, 19 (1976)

[14] I. Dutt and R. K. Puri, Phys. Rev. C **81**, 064609 (2010)

[15] S. Q. Yan, X. Y. Li, K. Nishio *et al*., Astrophys. J. **919**, 84 (2021)

[16] M. H. Macfarlane and S. C. Pieper. Technical Report ANL-76-11 (Rev. 1), Argonne National Laboratory, 1978

[17] T. Kammuri and H. Yoshida, Nucl. Phys. A **129**(3), 625 (1969)

[18] J. Vernotte, G. Berrier-Ronsin, J. Kalifa *et al*., Nucl. Phys. A **571**(1), 1 (1994)

[19] J. England, T. Ophel, R. Bark *et al*., Nucl. Phys. A **470**(1), 241 (1987)

[20] M. S. Child, *Semiclassical methods in molecular scattering and spectroscopy: proceedings of the NATO ASI held in Cambridge, England, in September 1979* (Dordrecht: Springer Science & Business Media, 2012), p. 42

[21] J. B locki, J. Randrup, W. J. Światecki *et al*., Ann. Phys. **105**, 427 (1977)

[22] L. C. Chamon, B. V. Carlson and L. R. Gasques, Comput. Phys. Commun. **267**, 108061 (2021)